



Internal regulation in compressible turbulent shear layers

K. Matsuno¹ and S. K. Lele^{1,2,†}

¹Department of Mechanical Engineering, Stanford University, Stanford, CA 94305, USA

²Department of Aeronautics & Astronautics, Stanford University, Stanford, CA 94305, USA

(Received 9 July 2020; revised 14 September 2020; accepted 17 October 2020)

High-resolution simulations of temporally evolving mixing layers, for convective Mach numbers ranging from $M_c = 0.2$ to $M_c = 2.0$ with density ratios $s = 1$ and $s = 7$, are analysed to characterize compressibility effects on the structure and evolution of turbulence in this compressible flow. Published experimental results are used to validate simulation results. Examination of the turbulence scales in the present data suggests an internal regulation mechanism. Correlated eddying motions were found to be in support of a ‘sonic eddy hypothesis’. Eddy scales in all spatial directions are found to be a progressively smaller fraction of the overall mixing-layer thickness with increasing M_c , forming independent layers of eddying motions at high M_c . These reduced spatial scales serve to reduce the effective velocity scale for turbulent motions, suppressed Reynolds stresses, turbulent kinetic energy (TKE) production and dissipation, and the mixing-layer thickness growth rate.

Key words: shear layer turbulence, compressible turbulence, turbulence simulation

1. Introduction

Compressible turbulent mixing plays a key role in many diverse applications from high-speed propulsion, supernova dynamics, interstellar turbulence and inertial-confinement fusion (Dimotakis 1991; Andrews 2011). In compressible mixing layers, a well-known compressibility effect manifests as a suppressed growth rate; this has been demonstrated numerous times in both experiment and direct numerical simulation (DNS) (Brown & Roshko 1974; Papamoschou & Roshko 1988; Lele 1989; Sandham & Reynolds 1991; Rossmann, Mungal & Hanson 2001). This stabilization has been confirmed to result from compressibility effects rather than density effects, though Clemens & Mungal (1995) showed that flow compressibility has quantifiable effects on the mass fraction fluctuations. It is widely recognized that the dominant compressibility effect is

† Email address for correspondence: lele@stanford.edu

evident in the pressure-strain correlation (Sarkar 1995; Vreman, Sandham & Luo 1996; Pantano & Sarkar 2002). Several models have been proposed to capture the consequences of compressibility on turbulence in shear flows (Kim 1990; Cambon, Coleman & Mansour 1993; Sarkar 1995; Adumitroaie, Ristorcelli & Taulbee 1999; Gomez & Girimaji 2013, 2014). Aupoix (2004) presented a comprehensive review of Reynolds-averaged Navier–Stokes models for compressible mixing layers.

While these models succeed in capturing the gross statistics, *viz.* averaged velocity profiles and reduced growth rates, current theory explaining these reduced growth rates and other observed changes remain somewhat incomplete. A comprehensive theory regarding high-Mach-number alterations to turbulence structure has remained elusive. Vreman *et al.* (1996) reported simulation results for compressible shear layers up to $M_c = 1.2$ (with M_c defined in (1.1a–d)) and introduced a relationship between growth rates and pressure extrema. From the integrated equations for the Reynolds stress tensor, Vreman *et al.* (1996) conclude that reduced pressure fluctuations act via the pressure-strain term to reduce growth rates. They also formulated a model for pressure fluctuation reduction informed by the sonic eddy hypothesis by Breidenthal (1992), and showed good agreement. Breidenthal’s hypothesis of sonic eddy communication is conceptually related to acoustic limitations on rotational velocity induced by vortices (Papamoschou & Lele 1993). Burr & Dutton (1990) also considered communication in terms of pressure wave propagation as the definition for a representative eddy length scale. Pantano & Sarkar (2002) affirmed the importance of pressure-strain reduction and showed that time delays associated with the finite speed of sound in highly compressible flows reduce the correlation between fluctuating pressure and fluctuating strain rate. They also showed that the gradient Mach number is a key parameter in pressure-strain rate reduction. Freund, Lele & Moin (2000) analysed the trends in turbulent kinetic energy (TKE) budgets, length scales and time scales at increasing M_c from simulation of an annular round jet. More recently, near-field pressure fluctuations including Mach wave emission from supersonic mixing layers up to M_c of 1.75 have been studied in Buchta, Anderson & Freund (2014) and Buchta & Freund (2017). Studies of the topology of the turbulent/non-turbulent interface of mixing layers with increasing compressibility have detailed decreased entrainment and mass and enstrophy transport across the interface (Jahanbakhshi & Madnia 2016, 2018). These investigations provide further insight into compressible shear-layer behaviour but several open questions remain.

The present work is intended to investigate the asymptotic effects of compressibility on the structure and scales of turbulence in the high-Mach-number regime. Turbulent statistics for compressible mixing layers over convective Mach numbers $M_c = [0.2, 0.4, 0.8, 1.2, 1.6, 2.0]$ with density ratio $s = 1$, and a set of cases at $M_c = [0.2, 0.8, 2.0]$ with density ratio $s = 7$ are used. Results on shear layer growth rates and turbulent stresses are first validated against published data. Further analysis of results in the self-similar regime provides insights into turbulent structures in this comprehensive parameter space. At high M_c , the energy-containing eddies do not span across the overall shear-layer thickness. Their spatial scale and intensity appear to be internally regulated and suggest an alternative scaling for the Reynolds stresses, turbulence budgets and growth rates. This paper focuses on this evidence and the internal scaling based on the effective velocity difference seen by the eddies. The results are interpreted in relation to the ‘multi-layered’ mixing proposed by Planché & Reynolds (1992) and Day, Reynolds & Mansour (1998), and the sonic eddy hypothesis by Breidenthal (1992).

Internal regulation in shear layers

1.1. Physical parameters

The upper free stream has density ρ_1 , speed of sound $c_1 = \sqrt{\gamma p_0/\rho_1}$, where γ is a constant ratio of specific heats, p_0 is a constant pressure value, and velocity $u_1 = \Delta\bar{u}/2$. The lower free stream has a density ρ_2 , speed of sound $c_2 = \sqrt{\gamma p_0/\rho_2}$ and velocity $u_2 = -\Delta\bar{u}/2$. The convective Mach number M_c and the density ratio s , which quantify the compressibility and the density variation in the flow, and two common Reynolds numbers are defined below with kinematic viscosity ν . (Notation: $^\circ$ indicates an initial value; $\bar{\cdot}$ and \prime indicate planar (x and z) averages and fluctuations; $\tilde{\cdot}$ and $\prime\prime$ indicate Favre averages and fluctuations.)

$$M_c = \frac{\Delta\bar{u}}{c_1 + c_2}, \quad s = \frac{\rho_2}{\rho_1}, \quad Re_\theta^\circ = \frac{\Delta\bar{u}\delta_\theta^\circ}{\nu}, \quad Re_\omega^\circ = \frac{\Delta\bar{u}\delta_\omega^\circ}{\nu}. \quad (1.1a-d)$$

The vorticity thickness δ_ω and the momentum thickness δ_θ , used above, are two key measures of mixing-layer thickness. The 99% thickness, δ_{99} , is a measure of the overall thickness (transverse scale) of the flow. These length scales grow in time and remain small compared to the height of the computational domain L_y , where $y \in [-L_y/2, L_y/2]$.

$$\delta_{99}(t) = \delta_1 + \delta_2 \quad \text{with} \quad \frac{\bar{u}(\delta_1)}{\Delta\bar{u}/2} = 0.99, \quad \frac{\bar{u}(-\delta_2)}{\Delta\bar{u}/2} = -0.99, \quad (1.2)$$

$$\delta_\omega(t) = \frac{\Delta\bar{u}}{|d\bar{u}/dy|_{\max}}, \quad (1.3)$$

$$\delta_\theta(t) = \frac{1}{\rho_0(\Delta\bar{u})^2} \int_{-L_y/2}^{L_y/2} \bar{\rho} \left(\frac{1}{2}\Delta\bar{u} - \tilde{u}_1 \right) \left(\frac{1}{2}\Delta\bar{u} + \tilde{u}_1 \right) dy. \quad (1.4)$$

Previous DNS studies of this problem (see [table 1](#)) have presented results for convective Mach numbers up to $M_c \leq 1.8$, but at lower Reynolds numbers $O(Re_\theta^\circ) \sim 100$ ([Vreman et al. 1996](#); [Pantano & Sarkar 2002](#)). Previously published data are also insufficient to clearly isolate compressibility effects from density effects over the full range of M_c . [Pantano & Sarkar \(2002\)](#) studied compressibility effects in shear layers up to $M_c = 1.2$ and variable density effects at a single $M_c = 0.7$. The density effects have not yet been explored across a large range of M_c . The present simulations also address this gap in knowledge.

[Table 2](#) gives the complete suite of cases presented in this work. Each case is run with the same initial thicknesses $\delta_\theta^\circ = 1$ (corresponding to $\delta_\omega^\circ = 4$), and continued until $\delta_\theta \sim 3.5$. The initial Reynolds number $Re_\theta^\circ = 1000$, Prandtl number $Pr = 0.7$, and Schmidt number $Sc = 1$ are also the same for all cases. The initial density profiles, set by s , and the velocity profile with free stream values of $\pm\Delta\bar{u}/2$ are given below.

$$\bar{u}(y) = \frac{\Delta\bar{u}}{2} \tanh\left(\frac{y}{2\delta_\theta^\circ}\right), \quad \bar{\rho}(y) = \rho_0 \left[1 + \frac{s-1}{s+1} \tanh\left(\frac{y}{2\delta_\theta^\circ}\right) \right]. \quad (1.5a,b)$$

1.2. Numerical methods

The continuity equation for species mass fractions and the Navier–Stokes equations for momentum and total energy in the compressible flow of an ideal gas are solved. Spatial derivatives are computed with 10th-order compact finite difference schemes ([Lele 1992](#))

Study	M_c	Re_θ°	Re_θ	Re_ω	$\eta/\Delta x$
Pantano & Sarkar (2002)	1.1	160	1760	13 640	0.380
Vaghefi (2014)	1.8	N/A	N/A	16 800	1.322
Buchta & Freund (2017)	1.75	60	2100	N/A	N/A
Arun <i>et al.</i> (2019)	1.2	160	2080	11 112	0.465
Matsuno & Lele (2020) (present work)	2.0	1000	3800	18 480	0.409

TABLE 1. A brief comparison of key flow parameters with previous studies. N/A indicates ‘not available’. A complete table of previous studies is given by Matsuno & Lele (2020) where the resolution of viscous scales is also discussed.

Case	M_c	s	$\frac{1}{\delta_\theta^\circ}(L_x \times L_y \times L_z)$	$\frac{1}{\delta_\theta^\circ}(\Delta x \times \Delta y \times \Delta z)$
A1	0.2	1	$150 \times 200 \times 75$	$0.146 \times 0.138 \times 0.146$
A7	0.2	7	$150 \times 200 \times 75$	$0.146 \times 0.138 \times 0.146$
B1	0.4	1	$150 \times 200 \times 75$	$0.146 \times 0.138 \times 0.146$
C1	0.8	1	$100 \times 100 \times 50$	$0.098 \times 0.069 \times 0.098$
C7	0.8	7	$100 \times 100 \times 50$	$0.098 \times 0.069 \times 0.098$
D1	1.2	1	$100 \times 100 \times 50$	$0.098 \times 0.069 \times 0.098$
E1	1.6	1	$80 \times 80 \times 40$	$0.078 \times 0.055 \times 0.078$
F1	2.0	1	$80 \times 80 \times 40$	$0.078 \times 0.055 \times 0.078$
F7	2.0	7	$80 \times 80 \times 40$	$0.078 \times 0.055 \times 0.078$

TABLE 2. Parameters, domains and grid resolutions for cases studied. All cases use uniformly spaced grid points in the x , y and z directions of $N_x \times N_y \times N_z = 1024 \times 1448 \times 512$.

and the system is time advanced with a low-storage 4th-order Runge–Kutta scheme. An 8th-order compact filter for dealiasing is applied for spatial derivatives at the end of each time step. Each species follows the ideal gas equation of state, and has the same ratio of specific heats $\gamma_1 = \gamma_2 = 1.4$. Details on interspecies mixing rules can be found in Subramaniam (2018). Initial perturbations for the $M_c = 0.2$ cases follow the random mode potential perturbations outlined in Kleinman & Freund (2008). Higher M_c cases are initialized from turbulent $M_c = 0.2$ fields at time $t = 60$.

2. Compressibility effects on turbulent structure and high-Mach regime

2.1. Growth rates and turbulent stresses

The temporal evolution of the momentum thickness becomes linear after an initial period of transition. As depicted in figure 1(a), this constant rate of growth decreases monotonically with increasing M_c . Intersecting tick marks indicate the duration of self-similar regime, which is determined from collapse of the Reynolds shear stress profiles $R_{12} = u''v''$. All error bars presented in this study represent temporal variations from the average value in this self-similar regime. Examples of this collapse and temporal variability are demonstrated in Matsuno & Lele (2020).

Figure 1(b) shows the well-known departure from the incompressible growth rate δ_{inc} , with $\delta_{inc} = 0.018, 0.013$ (Pantano & Sarkar 2002) for $s = 1, 7$ cases, respectively. A drastic

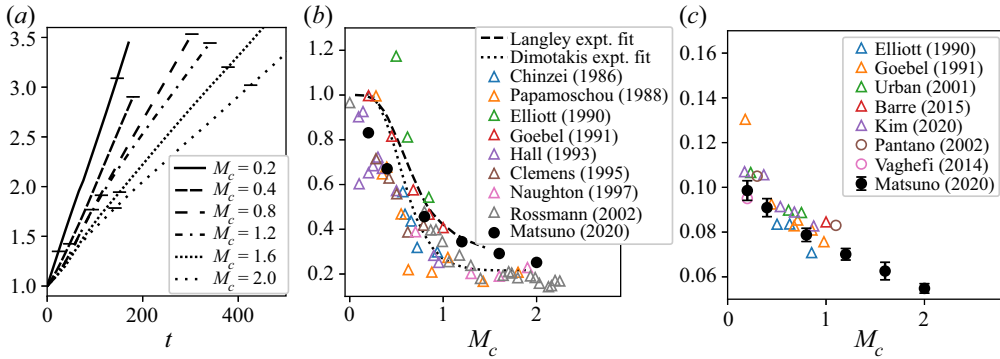


FIGURE 1. Growth rates and shear stress with increasing M_c : (a) evolution of $\delta_\theta(t)$; (b) normalized growth rates $\hat{\delta}_\theta/\hat{\delta}_{inc}$ (c) peak turbulent shear stress magnitudes $\sqrt{|R_{12}|}/\Delta\bar{u}$ with numerical simulation data plotted with open circles. Present results for $s = 1$ are shown with filled circles.

reduction occurs near $M_c \sim 0.5$, followed by an asymptotic approach to a normalized growth rate $\hat{\delta}_\theta/\hat{\delta}_{inc} \approx 0.2$. Our computed growth rates for the cases with unity density ratio show good agreement with well-known experimental results. Peak magnitudes of Reynolds stresses $R_{ij} = \overline{u'_i u'_j}$ are also consistent with previously published experimental results at lower M_c , and figure 1(c) indicates that turbulent shear stress magnitude continues to decrease with increasing M_c . While the reduction across M_c is not of the same magnitude as the reduction of the momentum thickness growth rate, the decrease in this shear stress confirms that the velocity fluctuations driving the spread of the mixing layer are decreasing in a manner consistent with the growth rates.

Visualizations of transverse velocity across the mixing layer are shown for the lowest and highest M_c cases in figure 2. The domains (truncated for visual comparison) are scaled by the total mixing-layer thickness δ_{99} to allow for a direct comparison of eddy length scales. The scale disparity between the two cases is qualitatively obvious; in the next section, the turbulence scales are discussed quantitatively and used to propose an alternative explanation for growth rate reduction.

3. Turbulence length and time scales

In addition to the thickness measures δ_{99} , δ_ω and δ_θ , which characterize the mean velocity profile, a decorrelation length scale is used to characterize the effect of increasing M_c on the energy-containing scales. This length scale, δ_y , is defined in (3.1) using a pair of points symmetrically placed around an anchor point y_0 at a mutual separation distance of δ_y . A decrease in the correlation to 0.1 is used to define this length scale, with the anchor point $y_0 = y_c$ at the shear-layer centre, where $\tilde{u}(y_c) = 0$.

$$\frac{v'(y_0 - \delta_y/2)v'(y_0 + \delta_y/2)}{v'(y_0)v'(y_0)} = 0.1. \tag{3.1}$$

This length scale as a fraction of total mixing-layer thickness decreases significantly from the quasi-incompressible case at $M_c = 0.2$ to the highly compressible case at $M_c = 2.0$. Figure 3(a) shows the transverse correlation length for the fluctuating transverse velocity and the effect of shifting the anchor point to $y_c \pm \delta_{99}/4$. Present data indicates a threefold

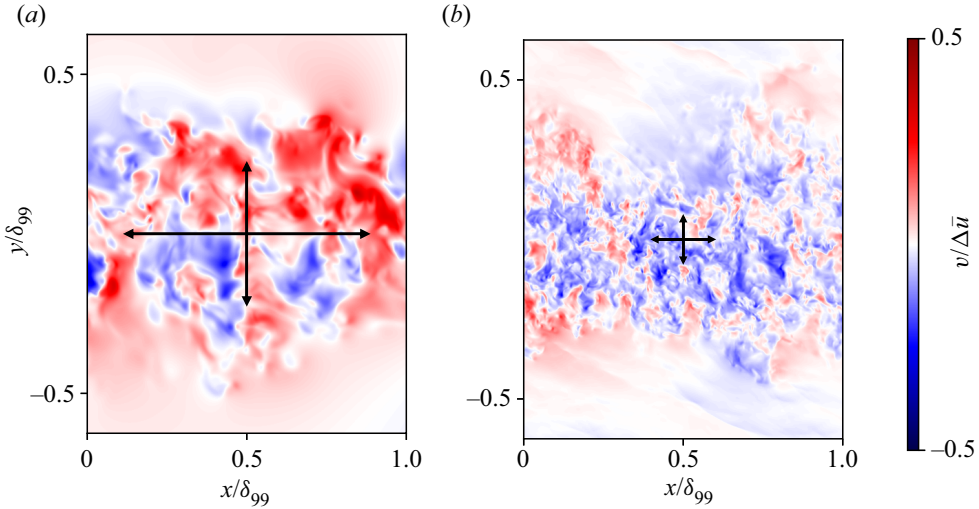


FIGURE 2. Instantaneous planar view (x - y plane) at $z = L_z/2$ slices of transverse velocity v at final simulation time for (a) $M_c = 0.2$ and (b) $M_c = 2.0$ cases. Arrows indicate decorrelation length scales based on v' along x and y axes.

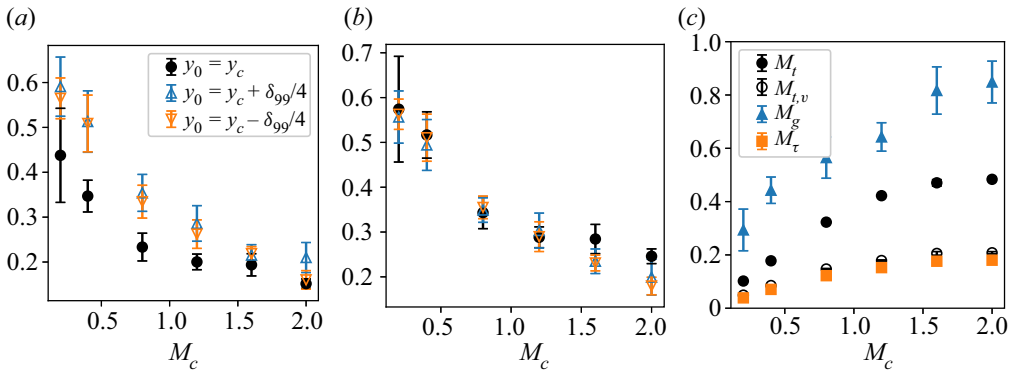


FIGURE 3. Effect of compressibility on (a) normalized decorrelation lengths δ_y/δ_{99} for v' measured about different y_0 , (b) mean velocity difference $U_\delta/\Delta\bar{u}$ across the v' decorrelation length, and (c) various Mach numbers.

decrease (from low to high M_c) in δ_y along the centreline, and nearly a fourfold decrease in δ_y for points offset from the centreline. Figure 3(a) also indicates that δ_y measured about y_c is the minimum decorrelation length in the mixing layer at each M_c . The occurrence of minimum length scale is intuitive since maximum shear also occurs along the centreline.

The mean velocity difference across the average decorrelation length scale centred about anchor point y_0 , defined as U_δ in (3.2), is also an important turbulent statistic of these eddies. The behaviour of this velocity scale, plotted in 3(b), matches the familiar reduction of normalized growth rates shown in figure 1(b).

$$U_\delta = \tilde{u} \left(y_0 + \frac{\delta_y}{2} \right) - \tilde{u} \left(y_0 - \frac{\delta_y}{2} \right). \quad (3.2)$$

The time scales of turbulent motions are also inherently linked to the reported decorrelation length scales δ_y . The most obvious time scale of interest is that of the acoustic scale set by the mean speed of sound $\bar{c} = \sqrt{\gamma p/\rho}$, which effectively defines the reach of acoustic communication in a mean sense. A second time scale to consider is the one associated with eddy distortion due to the shearing of the mean flow, which corresponds to the centreline (maximum) shear $S = d\bar{u}/dy$. Finally, the turbulent time scales associated with the turbulent velocity fluctuations and shear stresses are considered. In this discussion, these time scales are also interpreted as the Mach numbers defined below.

$$M_t = \frac{\sqrt{\overline{u''_i u''_i}}}{\bar{c}} \Big|_{y_c}, \quad M_{t,v} = \frac{\sqrt{\overline{v'' v''}}}{\bar{c}} \Big|_{y_c}, \quad M_\tau = \frac{\sqrt{\overline{|u'' v''|}}}{\bar{c}} \Big|_{y_c}, \quad M_g = \frac{S\delta_y}{\bar{c}} \Big|_{y_c}. \tag{3.3a-d}$$

The turbulent Mach numbers, M_t , represent the ratio of the mean acoustic time scale to the time scale of turbulent fluctuations. As shown in figure 3(c), while M_t shows saturation at the highest M_c , the turbulent Mach number defined using only the transverse component of TKE, $M_{t,v}$, indicates saturation at lower levels of compressibility, as further evidence for the pronounced effect of compressibility on the fluctuating transverse velocity. Freund *et al.* (2000) showed the beginning of a saturated regime for these time scale ratios for an annular mixing layer. The present M_t and $M_{t,v}$ show this trend at higher M_c in a self-similar shear layer. A friction Mach number, M_τ , of the turbulent mixing layer can be defined using the turbulent shear stress. In the present simulations, $M_\tau \leq 0.5$. Even at the lowest M_c cases, M_τ remains much larger than the M_τ encountered in turbulent boundary layers of high-speed, compressible flows (Bradshaw 1977). As a complement to the M_τ description of turbulent shear, the gradient Mach number, M_g , describes the compressibility effect of mean shear. The gradient Mach number represents the ratio of the acoustic time scale to the mean deformation time scale. Unlike M_t , this time scale ratio does not show a clear plateau although such a tendency is suggested by the data. Studies at even higher M_c are required to fully demonstrate this saturation.

Even in the most compressible case, each of the Mach numbers investigated in figure 3(c) remain subsonic. The sonic eddy hypothesis, as proposed by Breidenthal (1992), would suggest that since acoustic communication across these eddies is possible, these eddies remain coherent and participate in entrainment. Present data indicates that in the M_c range of significant growth rate reduction, the energy-containing eddies are subsonic. Assuming that eddies of scale δ_y are active in entrainment, the relative shear across these eddies appears directly related to the growth rate behaviour. At lower M_c , these eddies span across a large portion of the overall mixing-layer thickness, whereas at high M_c , the mixing layer consists of several ‘colayers’ of energy-bearing eddies. Figure 4 indicates that several autocorrelation profiles can fit within the mixing-layer thickness at $M_c = 2.0$, and that this structure is consistently maintained during the self-similar regime. Such behaviour suggests an internal regulation mechanism which limits the formation of still larger scales in the higher M_c mixing layers.

From figure 3(c), the turbulent Mach number M_t and transverse turbulent Mach number $M_{t,v}$ reach a plateau of approximately 0.5 and 0.2, respectively. The latter suggests that sound has sufficient time to ricochet 2–3 times across the transverse correlation scale during eddy turnover. Motions at still larger scales are evidently unable to remain coherent. They may correspond to acoustic response, but not rotational eddies. Figure 5(a) shows the ratio of correlation scales along x and y directions, δ_x/δ_y , and along the z and y directions,

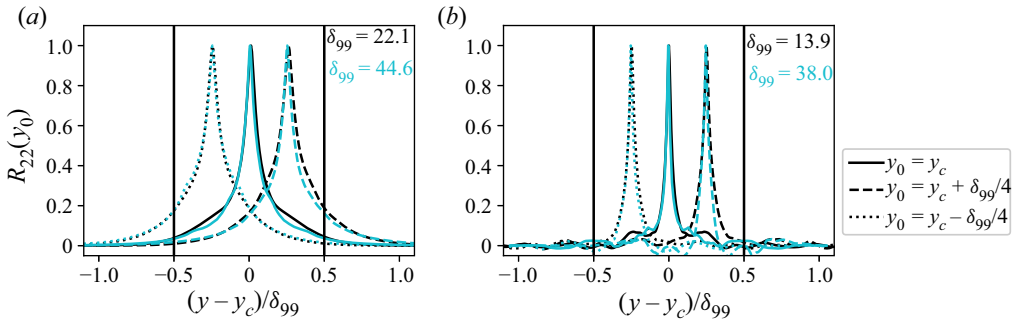


FIGURE 4. Autocorrelation profiles $R_{22}(y_0)$ for v' measured about different y_0 for (a) $M_c = 0.2$ and (b) $M_c = 2.0$ at the beginning (black) and end (blue) of self-similar spreading. Overall mixing-layer thickness δ_{99} is indicated in terms of initial thickness δ_θ^0 .

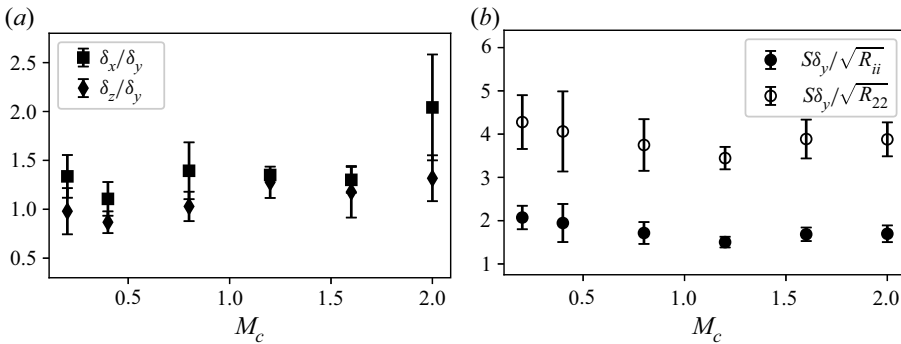


FIGURE 5. (a) Decorrelation ratios and (b) dimensionless shear (Corrsin number).

δ_z/δ_y against M_c (a data processing error invalidates the corresponding plot in Matsuno & Lele (2020)). Note that these ratios are relatively constant (the $M_c = 2.0$ point is an outlier since it may be affected by the smaller domain size in x). The internal regulation mechanism which limits the transverse scale to a decreasing fraction of the total shear-layer thickness δ_{99} also limits the correlation scales in the x and z directions and maintains approximately the same ratio in correlation scales. All of these trends are consistent with acoustic communication as the regulation mechanism for maintaining coherent eddying motions. Figure 5(b) shows the dimensionless shear number, or Corrsin number, $S\delta_y/\sqrt{R_{ii}} = M_g/M_t$ and $S\delta_y/\sqrt{R_{22}} = M_g/M_{t,v}$ against M_c , with $R_{ii} = \overline{u'_i u'_i}$ and $R_{22} = \overline{v'' v''}$. These measures are relatively constant with M_c , which affirms that the regulation is not associated with an increased importance of shear with M_c , but with acoustic communication limiting the turbulence length scales in the flow.

4. Scaling of Reynolds stress, turbulent production and growth rates

Profiles of Reynolds shear stress magnitudes $|R_{12}| = \overline{|u'v'|}$ scaled using the total velocity difference $\Delta\bar{u}$ and the effective velocity scale U_δ are shown in figure 6. Whereas scaling using $\Delta\bar{u}$ indicates a steady decline in $|R_{12}|$, scaling using U_δ^2 results in a clear separation between Reynolds stress profiles at low versus high M_c . Turbulent shear stresses

Internal regulation in shear layers

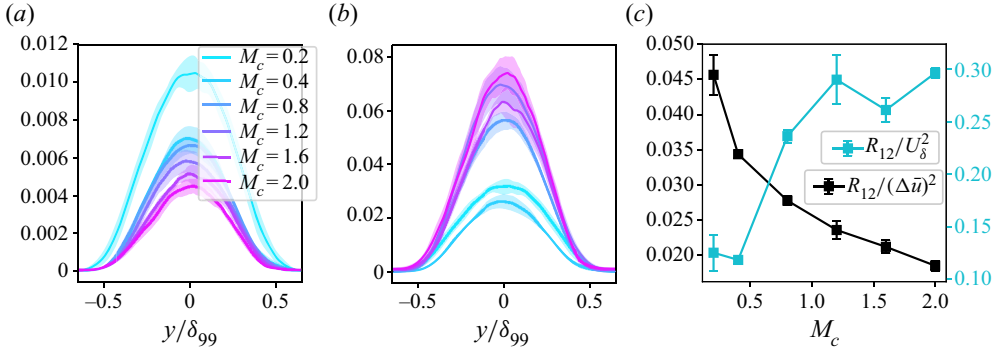


FIGURE 6. Turbulent shear stress: (a) $|R_{12}|/(\Delta\bar{u})^2$; (b) $|R_{12}|/U_\delta^2$; (c) integrated $|R_{12}|$ vs. M_c .

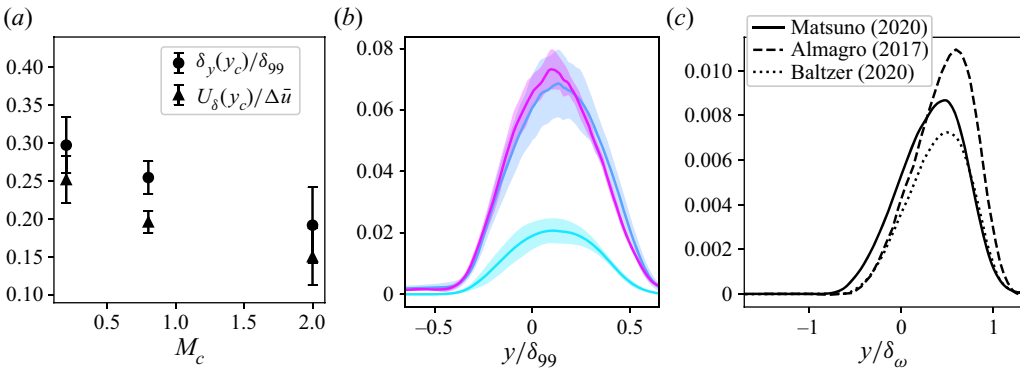


FIGURE 7. Scaling for $s = 7$ cases: (a) decorrelation scales δ_y and U_δ ; (b) $|R_{12}|/U_\delta^2$; (c) $|R_{12}|/(\Delta\bar{u})^2$ at $M_c = 0.2$ compared to recent literature for $M_c \rightarrow 0$.

scaled by $\Delta\bar{u}$ reported by Almagro, García-Villalba & Flores (2017) at $s = 8$ and Baltzer & Livescu (2020) at $s = 7$ with $M_c \rightarrow 0$ are compared to our quasi-incompressible case, $M_c = 0.2$, in figure 7(c) as confirmation that the variable density stresses are within the range of comparable studies. The scaling for $s = 7$ cases is similar to that of the $s = 1$ cases. The internal length scale δ_y and effective velocity scale U_δ in figure 7(a) follow similar declines to those in figures 3(a) and 3(b). Figure 3(b) shows the same scaling in 6(b) applied to $|R_{12}| = |u''v''|$ for $s = 7$ cases. A similar separation arises between the low and high M_c cases, and the high M_c cases attain scaled magnitudes close to those in the $s = 1$ cases.

Similarly, TKE production and dissipation may be scaled using either the overall mixing-layer scales or the internal scales associated with transverse velocity decorrelation. Figure 8 shows integrated TKE production P , TKE dissipation D , and pressure-strain component $\Pi_{11} = 2\overline{p'(du''/dx)}$, which acts to transfer energy out of $R_{11} = \overline{u''u''}$, scaled by $\delta_{99}/(\Delta\bar{u})^3$ and δ_y/U_δ^3 . The production term is related to the growth rate definition offered by Vreman *et al.* (1996), such that the values plotted in figure 8(a) represent $\delta_\theta \times \rho_\infty \delta_{99}/(2\delta_\theta \Delta\bar{u})$. Dissipation normalized with internal scales transforms the trend of progressive decrease of the quantity with M_c to an approximately constant value for $M_c > 0.2$. Internally scaled production and pressure-strain Π_{11} show a similar asymptotic behaviour past $M_c \sim 0.8$. The asymptotic approach towards constant

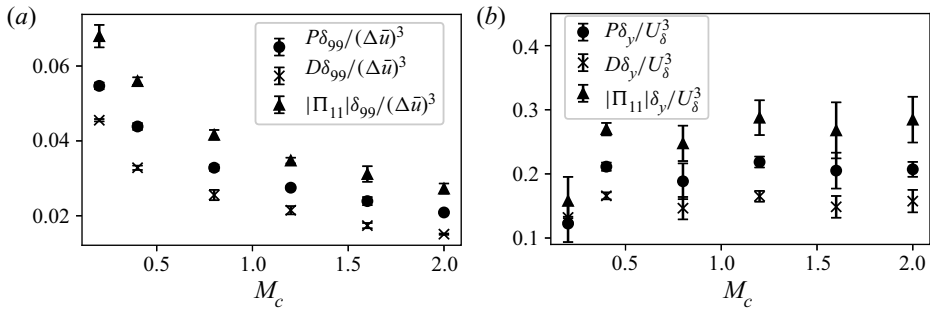


FIGURE 8. Selected TKE budget terms, integrated and scaled with (a) total thickness δ_{99} and total velocity difference $\Delta \bar{u}$ and with (b) internal scales δ_y and U_δ .

production, pressure-strain and dissipation, as well as evidence for constant turbulent shear stress magnitudes using the effective velocity scale U_δ further suggests the importance of δ_y as the defining length scale associated with turbulent mixing. This distinction may improve length-scale-based turbulence models.

5. Conclusion

In this work, the scales governing the turbulent structures in mixing layers with notable compressibility and density effects are thoroughly characterized. It is confirmed that as M_c increases, turbulence length scales, including the transverse length scale, reduce dramatically as a fraction of the overall shear-layer thickness. These length scales appear to be limited by acoustic communication; turbulence-associated Mach number(s) show saturation at higher levels of compressibility. The internal regulation adapts the spatial and temporal scales of shear-layer turbulence inferred from two-point correlations. It reduces the effective velocity scale, suppresses pressure fluctuations and mixing-layer growth rate. To accurately capture the effects of compressibility in free shear flows, turbulence models should capture not only the increasing anisotropy of turbulent stresses, but also the reduction in the turbulence length scales.

Acknowledgements

Simulations are supported by US Department of Energy Office of Science INCITE allocation 4978-4846 and through Argonne Leadership Computing Facility Director's Discretionary allocation 6195-6063. K.M. is funded by the NSF GRFP (National Science Foundation Graduate Research Fellowship Program). S.K.L. acknowledges partial support from NSF CBET 1803378.

Declaration of interests

The authors report no conflict of interest.

References

ADUMITROAIE, V., RISTORCELLI, J. & TAULBEE, D. 1999 Progress in Favre–Reynolds stress closures for compressible flows. *Phys. Fluids* **11** (9), 2696–2719.

Internal regulation in shear layers

- ALMAGRO, A., GARCÍA-VILLALBA, M. & FLORES, O. 2017 A numerical study of a variable-density low-speed turbulent mixing layer. *J. Fluid Mech.* **830**, 569–601.
- ANDREWS, M. 2011 Workshop: research needs for material mixing at extremes. *Tech. Rep.* LA-UR-11-02565. Los Alamos National Lab.
- ARUN, S., SAMEEN, A., SRINIVASAN, B., & GIRIMAJI, S. S. 2019 Topology-based characterization of compressibility effects in mixing layers. *J. Fluid Mech.* **874**, 38–75.
- AUPOIX, B. 2004 Modelling of compressibility effects in mixing layers. *J. Turbul.* **5** (7), 1–17.
- BALTZER, J. & LIVESCU, D. 2020 Variable-density effects in incompressible non-buoyant shear-driven turbulent mixing layers. *J. Fluid Mech.* **900**, A16.
- BRADSHAW, P. 1977 Compressible turbulent shear layers. *Annu. Rev. Fluid Mech.* **9** (1), 33–52.
- BREIDENTHAL, R. 1992 Sonic eddy-a model for compressible turbulence. *AIAA J.* **30** (1), 101–104.
- BROWN, G. & ROSHKO, A. 1974 On density effects and large structure in turbulent mixing layers. *J. Fluid Mech.* **64** (4), 775–816.
- BUCHTA, D., ANDERSON, A. & FREUND, J. 2014 Near-field shocks radiated by high-speed free-shear-flow turbulence. In *20th AIAA/CEAS Aeroacoustics Conference, AIAA Paper 2014–3201*.
- BUCHTA, D. & FREUND, J. 2017 The near-field pressure radiated by planar high-speed free-shear-flow turbulence. *J. Fluid Mech.* **832**, 383–408.
- BURR, R. & DUTTON, J. 1990 Numerical modeling of compressible reacting turbulent shear layers. In *21st Fluid Dynamics, Plasma Dynamics and Lasers Conference, AIAA Paper 90–1463*.
- CAMBON, C., COLEMAN, G. & MANSOUR, N. 1993 Rapid distortion analysis and direct simulation of compressible homogeneous turbulence at finite mach number. *J. Fluid Mech.* **257**, 641–665.
- CLEMENS, N. & MUNGAL, M. 1995 Large-scale structure and entrainment in the supersonic mixing layer. *J. Fluid Mech.* **284**, 171–216.
- DAY, M., REYNOLDS, W. & MANSOUR, N. 1998 The structure of the compressible reacting mixing layer: insights from linear stability analysis. *Phys. Fluids* **10** (4), 993–1007.
- DIMOTAKIS, P. 1991 Turbulent free shear layer mixing and combustion. In *High Speed Flight Propulsion Systems*, vol. 137, pp. 265–340.
- FREUND, J., LELE, S. & MOIN, P. 2000 Compressibility effects in a turbulent annular mixing layer. Part 1. Turbulence and growth rate. *J. Fluid Mech.* **421**, 229–267.
- GOMEZ, C. & GIRIMAJI, S. 2013 Toward second-moment closure modelling of compressible shear flows. *J. Fluid Mech.* **733**, 325–369.
- GOMEZ, C. & GIRIMAJI, S. 2014 Explicit algebraic reynolds stress model (earsm) for compressible shear flows. *Theor. Comput. Fluid Dyn.* **28** (2), 171–196.
- JAGANNATHAN, S. 2014 Reynolds and mach number scaling in stationary compressible turbulence using massively parallel high resolution direct numerical simulations. PhD thesis, Texas A&M University.
- JAHANBAKHSI, R. & MADNIA, C. 2016 Entrainment in a compressible turbulent shear layer. *J. Fluid Mech.* **797**, 564–603.
- JAHANBAKHSI, R. & MADNIA, C. 2018 Viscous superlayer in a reacting compressible turbulent mixing layer. *J. Fluid Mech.* **848**, 743–755.
- KIM, S. 1990 New mixing-length model for supersonic shear layers. *AIAA J.* **28** (11), 1999–2000.
- KLEINMAN, R. & FREUND, J. 2008 The sound from mixing layers simulated with different ranges of turbulence scales. *Phys. Fluids* **20** (10), 101503.
- LELE, S. 1989 Direct numerical simulation of compressible free shear flows. In *27th Aerospace Sciences Meeting, AIAA Paper 89–0374*.
- LELE, S. 1992 Compact finite difference schemes with spectral-like resolution. *J. Comput. Phys.* **103** (1), 16–42.
- MATSUNO, K. & LELE, S. 2020 Compressibility effects in high speed turbulent shear layers—revisited. In *AIAA Scitech 2020 Forum, AIAA Paper 2020–0573*.
- PANTANO, C. & SARKAR, S. 2002 A study of compressibility effects in the high-speed turbulent shear layer using direct simulation. *J. Fluid Mech.* **451**, 329–371.
- PAPAMOSCHOU, D. & LELE, S. 1993 Vortex-induced disturbance field in a compressible shear layer. *Phys. Fluids A* **5** (6), 1412–1419.
- PAPAMOSCHOU, D. & ROSHKO, A. 1988 The compressible turbulent shear layer: an experimental study. *J. Fluid Mech.* **197**, 453–477.

- PLANCHÉ, O. & REYNOLDS, W. 1992 Heat release effects on mixing in supersonic reacting free shear-layers. In *30th Aerospace Sciences Meeting and Exhibit, AIAA Paper 92-0092*.
- ROSSMANN, T., MUNGAL, M. & HANSON, R. 2001 Evolution and growth of large scale structures in high compressibility mixing layers. *J. Turbul.* **3**, N9.
- SANDHAM, N. D. & REYNOLDS, W. C. 1991 Three-dimensional simulations of large eddies in the compressible mixing layer. *J. Fluid Mech.* **224**, 133–158.
- SARKAR, S. 1995 The stabilizing effect of compressibility in turbulent shear flow. *J. Fluid Mech.* **282**, 163–186.
- SUBRAMANIAM, A. 2018 Simulations of shock induced interfacial instabilities including materials with strength. PhD thesis, Stanford University.
- VAGHEFI, S. J. 2014 *Simulation and Modeling of Compressible Turbulent Mixing Layer*. State University of New York at Buffalo.
- VREMAN, A., SANDHAM, N. & LUO, K. 1996 Compressible mixing layer growth rate and turbulence characteristics. *J. Fluid Mech.* **320**, 235–258.